Evaluation of Diffusion Tensor Imaging and Fiber Tractography of the Median Nerve: Preliminary Results on Intrasubject Variability and Precision of Measurements

Gustav Andreisek[1,2]
Lawrence M. White[1]
Andrea Kassner[3]
Marshall S. Sussman[4]

OBJECTIVE. The purposes of this study were to determine the intrasubject side-to-side variability of quantitative and qualitative measures of diffusion tensor imaging (DTI) and fiber tractography of the median nerves and to determine the precision of quantitative measurements and fiber tractography.

SUBJECTS AND METHODS. Fifteen healthy volunteers (seven men, eight women; mean age, 31.2 years) underwent DTI of both wrists with a single-shot spin-echo-based echo-planar imaging sequence (TR/TE, 7,000/103; b value 1,025 s/mm^2). Postprocessing included fiber tractography and quantitative analysis of fiber length, fiber density index, fractional anisotropy, apparent diffusion coefficient, and signal-to-noise ratio. Two readers in consensus graded the quality of fiber tract images of the two wrists as equal, slightly different, or very different. Fiber tractography and all analyses were repeated after 3 weeks, and the images from the two sessions were compared.

RESULTS. No statistically significant side-to-side differences in quantitative data were found (p = 0.054–0.999). In all subjects, the quality of fiber tract images of the right and left median nerves was either slightly or very different. Between the initial and the second quantitative analyses, no statistically significant differences (p = 0.086–0.898) were found, and the quality of fiber tract images was rated equal for nine of 15 subjects (60%) and slightly different for six of 15 subjects (40%).

CONCLUSION. Preliminary results indicate that quantitative evaluation of DTI of the median nerve is precise. The absence of statistically significant intrasubject side-to-side variability in quantitative data suggests that the healthy contralateral nerve can be used as an internal control. Observed side-to-side variability in the quality of fiber tract images, however, rules out side-to-side comparisons in fiber tractography.

Keywords: anisotropy, diffusion tensor imaging, fiber tractography, median nerve, peripheral neuropathy

DOI:10.2214/AJR.09.2517

Received February 2, 2009; accepted after revision July 8, 2009.

[1]Division of Musculoskeletal Imaging, Department of Medical Imaging, Mount Sinai Hospital and the University Health Network, University of Toronto, Toronto, ON, Canada.

[2]Department of Medical Radiology, Institute of Diagnostic Radiology, University Hospital Zürich, Rämistrasse 100, 8091 Zürich, Switzerland. Address correspondence to G. Andreisek (gustav@andreisek.de).

[3]Department of Medical Imaging, University Health Network, University of Toronto, Toronto, ON, Canada.

[4]Department of Medical Imaging, Toronto General Hospital, University of Toronto, Toronto, ON Canada.

WEB
This is a Web exclusive article.

AJR 2010; 194:W65–W72

0361–803X/10/1941–W65

Diffusion tensor imaging (DTI) is an emerging MRI method for gaining insight into tissue microstructure through monitoring of the random movement of water molecules, which is usually restricted in anisotropic tissues [1–5]. DTI typically shows signal attenuation in the direction of a magnetic field gradient applied in a distinct direction in 3D space. The degree of signal attenuation is proportional to the water diffusivity [6, 7]. The diffusion data can be used for quantitative diffusion metrics, such as apparent diffusion coefficient (ADC), a scalar value that reflects molecular diffusivity under motion restriction; fractional anisotropy (FA), a quantitative index used to characterize directional variability in diffusion; fiber density index; and fiber tractography, a method of visualizing DTI data. Fiber tractography is based on a line propagation technique in which a tracking line is propagated from a start point (seed) in the principal diffusion direction [1]. It can be used to track individual nerves or nerve bundles and to display them on color-coded 3D images [8–16].

Pilot studies have shown the feasibility of DTI and fiber tractography for imaging of peripheral nerve structures such as cervical nerve roots; the median and ulnar nerves at the wrist; the peroneal and tibial nerves at the knee, calf, and ankle; and the sciatic nerve [17–23]. To our knowledge, in only three studies [17, 23, 24] have normative quantitative diffusion data (i.e., ADC and FA) been collected on the median nerve. Such data may be important as a reference for clinical studies, such as those of patients with carpal tunnel syndrome [23]. In one of the three studies [17], however, the vari-

ability of ADC and FA data among subjects (intersubject variability) was found to be as high as 274%. Thus, there is a need for more robust reference data. We hypothesized that side-to-side variability in the same subject (intrasubject variability) might be lower than intersubject variability. Therefore, one of the purposes of this prospective cross-sectional study was to perform DTI and fiber tractography on both the left and right median nerves of 15 healthy volunteers to determine intrasubject side-to-side variability of quantitative and qualitative measures.

Studies of the brain have shown that DTI and fiber tractography depend on precise placement of regions of interest (ROIs) in which FA and ADC are calculated or that are used as seed ROIs for tracking of passing fibers [7, 25–28]. We sought to determine the precision of our measurements. We define precision as the same or similar results of repeated quantitative measurements and fiber tracking (based on the existing DTI data set) by the same operator. A second purpose of our study therefore was to determine the precision of quantitative measurements and fiber tractography.

Subjects and Methods

Study Subjects

This study was approved by the institutional research ethics board. Written informed consent was prospectively obtained from all study subjects. Fifteen healthy volunteers (seven men, eight women; mean age, 31.2 years; median age, 31.2 years; range, 22–44 years) participated. The inclusion criterion was age older than 18 years. Exclusion criteria were contraindications to MRI; pregnancy; and history of a cardiovascular, pulmonary, endocrine, metabolic, neurologic, neuromuscular, or musculoskeletal disorder.

MRI

MRI was performed with a 1.5-T system (Signa Excite HD, GE Healthcare) equipped with high-performance gradients (amplitude, 40 mT/m; slew rate, 200 T/m/s). A high-resolution eight-channel transmit–receive wrist coil was used. In all subjects, the left and right median nerves were imaged with a fat-suppressed single-shot spin-echo-based echo-planar imaging sequence (TR/TE, 7,000/103; matrix size, 64 × 64; field of view, 120 × 120 mm; slice thickness, 4 mm; number of slices, 22; acquisition time, 6 minutes 19 seconds; b value, 1,025 s/mm^2) [29]. Twenty-five diffusion-weighted direction-encoding images and one reference image without diffusion weighting were acquired per slice (Table 1). In addition, anatomic reference images were acquired with a standard transaxial T2-weighted fast spin-echo sequence (3,500/87; echo-train length, 11; matrix size, 256 × 224; field of view, 120 × 120 mm; slice thickness, 4 mm; number of slices, 22; acquisition time, 3 minutes 12 seconds) in identical slice locations.

Postprocessing With Fiber Tractography

One author (7 years of experience in MRI research) performed all image postprocessing and analysis. DTI software (dtiStudio release 2.4, Johns Hopkins University) was used. The same author, who was blinded to the initial results, repeated the image postprocessing and analysis 3 weeks after the initial session (Fig. 1).

For postprocessing, data sets were transferred to an independent workstation. Mean diffusion-weighted direction-encoding images (averaged over all 25 diffusion-weighted direction-encoding images) and FA and ADC maps were calculated (Fig. 2). A detailed description of these postprocessing procedures and of the software routines used has been previously published [16]. Fiber tractography was performed on an initial seed ROI at the level of the flexor retinaculum containing the median nerve. For selection of the ROI, the median nerve was identified from the standard anatomic reference MR images. An ROI slightly larger than the nerve diameter was drawn freehand and copied to the corresponding location on the DTI images [21]. Tracking of fibers included all voxels above an FA threshold of 0.1, allowing fiber angulation of up to 50°. Similar reconstruction parameters were used in previous studies [17, 22]. Representative fiber tract images were saved as TIFF files (Fig. 2F).

Quantitative Analysis of DTI Data

FA and ADC were calculated from oval ROIs placed in the center of the median nerve at the level of the flexor retinaculum (hook of hamate) [17]. To avoid partial volume artifacts, we made the ROIs slightly smaller than the cross-sectional area of the median nerve. We calculated the quantitative fiber density index, which describes the density of reconstructed fibers within an ROI [30], by dividing the number of reconstructed fibers traversing an individual ROI by the area of the ROI (in pixels).

Signal-to-Noise Ratio

It is known that calculation of quantitative data such as FA and ADC depends on the signal-to-noise ratio (SNR) of the DTI acquisition [7, 31]. A difference in SNRs in acquisition of images of the left and right median nerves (caused by differences in field homogeneity by slightly different subject and coil positions) can cause systematic underestimation or overestimation of FA and ADC. Thus we determined the SNR for all acquisitions using the following equation to allow direct side-to-side comparison of the SNRs of the acquisitions and hence of FA and ADC:

$$SNR = \frac{SI_{Nerve}}{SD_{Background\_noise}} \times \left(\sqrt{2-\frac{\pi}{2}}\right)$$

where SI_{Nerve} represents the mean signal intensity within an ROI (mean size, 0.1 cm^2) positioned in the center of the median nerve, and $SD_{Background\_noise}$ represents the average SD of the background noise within an ROI placed in the air outside the anatomic structure. For measurement of background noise, four standardized ROIs measuring 2 cm^2 were placed in four reproducible image locations outside the extremity and averaged for each wrist. A correction factor ($\sqrt{2-\varpi/2}$) was used to account for the systemic error in noise measurements in magnitude images [31, 32]. All ROI measurements

TABLE 1: Vectors for Diffusion-Weighting Directions

	Direction		
Index	*x*	*y*	*z*
1	1.000000	0.000000	0.000000
2	0.849000	0.528000	0.000000
3	−0.108000	0.565000	0.818000
4	0.884000	−0.345000	−0.315000
5	−0.003000	−0.736000	0.677000
6	−0.868000	−0.238000	0.436000
7	0.799000	0.370000	0.475000
8	−0.162000	0.987000	0.000000
9	0.866000	−0.129000	0.483000
10	−0.212000	−0.936000	0.281000
11	0.068000	−0.892000	−0.446000
12	0.550000	−0.544000	−0.634000
13	−0.435000	−0.422000	0.795000
14	−0.599000	0.780000	0.182000
15	−0.525000	0.030000	−0.851000
16	−0.600000	−0.688000	0.409000
17	0.653000	−0.060000	−0.755000
18	0.207000	−0.076000	−0.975000
19	−0.413000	−0.699000	−0.584000
20	−0.436000	0.822000	−0.366000
21	0.462000	0.874000	0.148000
22	−0.503000	0.488000	−0.713000
23	0.824000	−0.530000	0.202000
24	0.297000	0.349000	0.889000
25	−0.040000	0.318000	−0.947000

Note—Data needed to read and process diffusion-direction encoded MR images with dtiStudio software (release 2.4, Johns Hopkins University).

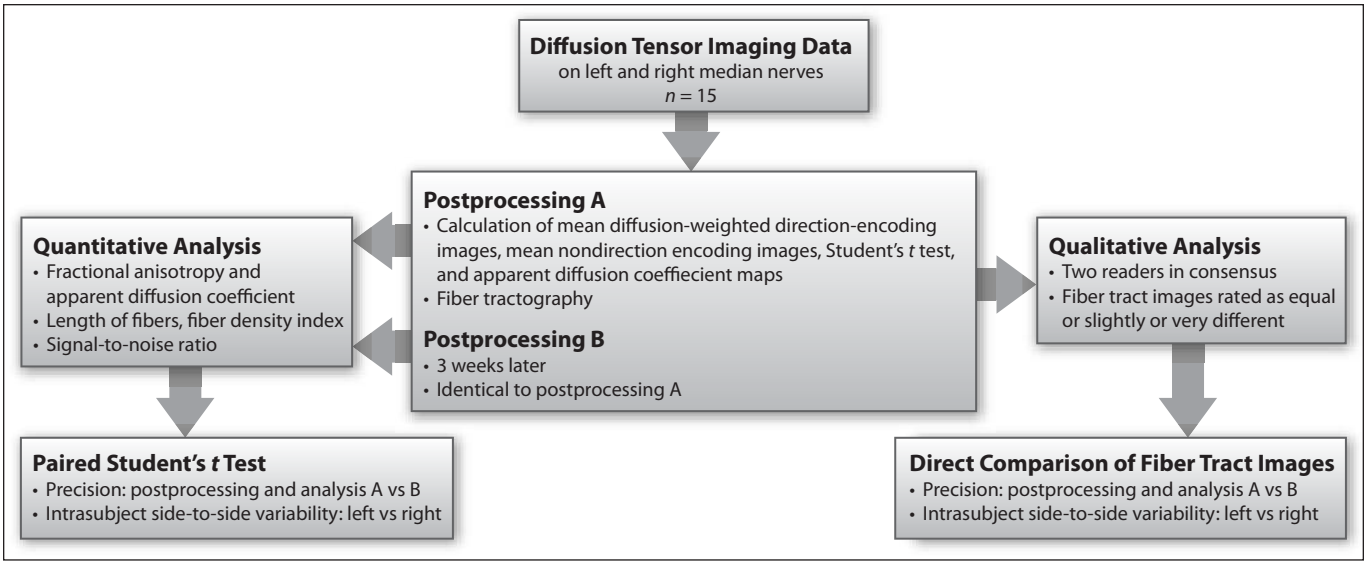

Fig. 1—Flow chart shows postprocessing and analysis of diffusion tensor imaging data on 15 healthy volunteers. Mean images and diffusion-related maps were calculated, and fiber tractography was performed. Quantitative data analysis was performed by calculation of fractional anisotropy, apparent diffusion coefficient, length of fibers, fiber density index, and signal-to-noise ratio. Image postprocessing with quantitative data analysis was repeated after 3 weeks by same operator, who was blinded to initial results. For qualitative image analysis, fiber tract images were evaluated by two readers in consensus.

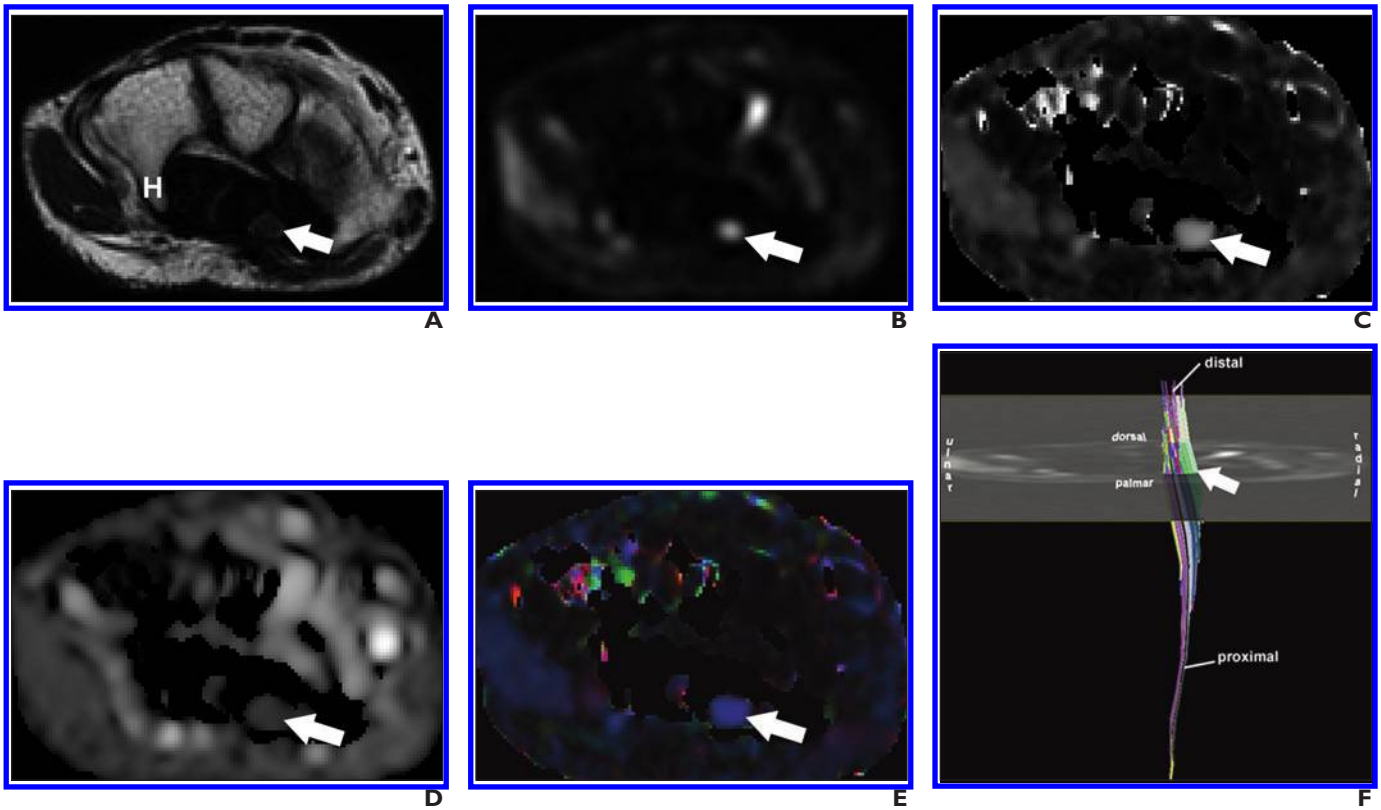

Fig. 2—29-year-old healthy woman.
A, Transaxial T2-weighted fast spin-echo MR image (TR/TE, 3,500/87; echo-train length, 11) of left wrist at level of flexor retinaculum shows anatomic reference features for identifying median nerve (*arrow*). H = hook of hamate.
B–E, Mean diffusion-weighted image (**B**), fractional anisotropy map (**C**), apparent diffusion coefficient map (**D**), and color-coded map combining information about magnitude of anisotropy and direction of principal eigenvector (**E**) show results of calculations from diffusion tensor imaging data set. Arrow indicates median nerve.
F, Oblique transaxial view of representative 3D fiber tract image generated from same diffusion tensor imaging data set as **B–E** shows reconstructed color-coded fiber tracts passing through seed region of interest (*arrow*).

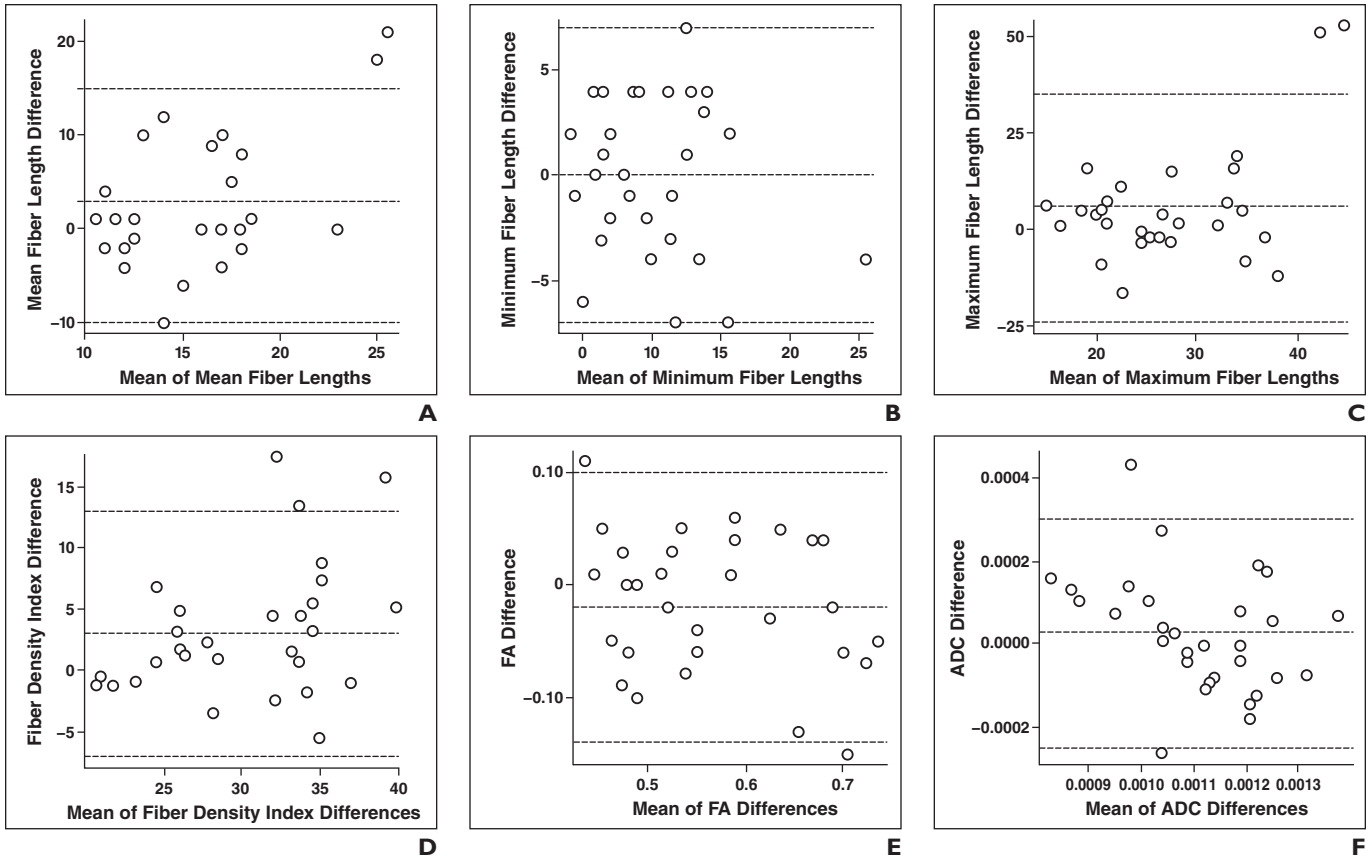

Fig. 3—Bland-Altman plots of comparisons of left and right median nerves. Neither systemic bias nor inadequate number of outliers is present. Most observed differences are within mean ± 1.96 SD. Horizontal dashed lines indicate mean difference (*middle line*) and limits of agreement, defined as mean difference plus (*upper line*) and minus (*lower line*) 1.96 × SD of differences.

A, Graph shows relation between differences in mean fiber lengths (mm) of left and right median nerves (*y*-axis) and means of mean fiber lengths of right and left median nerves (*x*-axis).

B, Graph shows relation between differences in minimum fiber lengths (mm) of left and right median nerves (*y*-axis) and means of minimum fiber lengths of right and left median nerves (*x*-axis).

C, Graph shows relation between differences in maximum fiber lengths (mm) of left and right median nerves (*y*-axis) and means of maximum fiber lengths of right and left median nerves (*x*-axis).

D, Graph shows relation between differences in fiber density indexes of left and right median nerves (*y*-axis) and means of fiber density indexes of right and left median nerves (*x*-axis).

E, Graph shows relation between differences in fractional anisotropy (FA) values of left and right median nerves (*y*-axis) and means of FA values of right and left median nerves (*x*-axis).

F, Graph shows relation between differences in apparent diffusion coefficients (ADCs) (× 10–3 mm^2/s) of left and right median nerves (*y*-axis) and means of ADCs of right and left median nerves (*x*-axis).

were performed on the transaxial mean diffusion-weighted direction-encoding images at the level of the flexor retinaculum (hook of hamate). The DTI software was used for all calculations.

Qualitative Image Analysis

Two readers (9 and 18 years of experience) were asked to assess all fiber tract images with regard to overall image quality. Image quality was based on findings at qualitative evaluation of fiber tract order and homogeneity, fiber tract organization, fiber length, appearance of fiber bundles in boundary regions, and apparent density of fiber bundles.

For the evaluation of the precision of the postprocessing operations, both readers were presented with the images reconstructed during the initial postprocessing and with corresponding images reconstructed during the second postprocessing 3 weeks later. In case of perfect precision between both postprocessing operations, image quality was expected to be equal. Thus both readers were asked to directly compare the corresponding images and to decide in consensus whether the images from the two postprocessing operations were equal, slightly different, or very different. Equal was defined as no obvious difference in fiber tract order, homogeneity, organization, or length or in appearance or apparent density of fiber bundles in the boundary regions. Slightly different was defined as differences in one or two of the aforementioned criteria. Very different was defined as differences in three or more criteria.

For evaluation of intrasubject side-to-side variability, the same approach and classification system were used as for the two postprocessing sessions. Both readers were presented with corresponding images of the left and right median nerves. In the absence of side-to-side variability, image quality was expected to be absolutely equal.

Statistical Analysis

Statistical analysis was performed by one author using statistical software (SPSS, version 12.0.1, SPSS). The Kolmogorov-Smirnov test was used to confirm normal distribution of quantitative data. The two-sided paired Student's *t* test was used to compare the mean, minimum, and maximum lengths of fibers and the FA, ADC, and fiber density index

TABLE 2: Differences Between Left and Right Median Nerves (Intrasubject Side-To-Side Variability) and Between Initial and Subsequent Image Postprocessing and Analysis Sessions (Precision of Measurements) (*n* = 15)

Comparison	Fiber Length (mm)			Fiber Density Index (mean ± SD)	Fractional Anisotropy (Mean ± SD)	Apparent Diffusion Coefficient ($\times 10^{-3}$ mm^2/s) (mean ± SD)
	Mean ± SD	Minimum ± SD	Maximum ± SD			
Initial postprocessing						
Left median nerve	17.4 ± 6.6	8.4 ± 3.9	27.2 ± 13.3	31.9 ± 6.7	0.56 ± 0.09	1.14 ± 0.13
Right median nerve	14.3 ± 4.2	8.3 ± 3.7	20.8 ± 8.0	29.5 ± 5.1	0.58 ± 0.10	1.09 ± 0.18
Difference of means	3.1 (21.7)	0.1 (1.2)	6.4 (30.8)	2.4 (8.1)	−0.02 (−3.5)	0.05 (4.6)
t test (left vs right)	0.096	0.948	0.125	0.054	0.162	0.197
Second postprocessing						
Left median nerve	16.8 ± 6.5	9.4 ± 3.1	26.2 ± 14.2	31.6 ± 7.3	0.56 ± 0.09	1.11 ± 0.12
Right median nerve	14.9 ± 4.1	9.4 ± 3.4	20.9 ± 8.0	28.1 ± 5.0	0.57 ± 0.12	1.11 ± 0.17
Difference of means	1.9 (2.6)	0 (0)	5.3 (25.4)	3.5 (12.5)	−0.01 (−1.8)	0 (0)
t test (left vs right)	0.307	0.999	0.204	0.056	0.605	0.867
First versus second postprocessing						
Left median nerve						
Difference of means	0.6 (3.6)	−1.0 (−10.6)	1 (3.8)	0.3 (1.0)	0 (0)	0.03 (2.7)
t test	0.144	0.224	0.136	0.586	0.454	0.096
Right median nerve						
Difference of means	0.6 (4.0)	−1.1 (−11.7)	−0.1 (−0.5)	1.4 (5.0)	0.01 (1.8)	−0.02 (−1.8)
t test	0.003	0.104	0.898	0.086	0.372	0.301

Note—Mean values and SD and differences of means between the left and right median nerves and between the first and second postprocessing operations are absolute numbers. Differences in means are accompanied by percentages (in parentheses) calculated as follows: mean difference percentage = (mean value $_{\text{left, first}}$ − mean value$_{\text{right, second}}$) / (mean value$_{\text{right, second}}$) × 100. Values of *p* for the side-to-side comparisons and for the first and second postprocessing comparisons are based on results of Student's *t* tests. A Bonferroni-adjusted level of $\alpha = 0.0016$ was considered indicative of significance.

values of the left and the right sides (intrasubject side-to-side variability) and of the initial and second postprocessing and quantitative analysis operations (precision of measurement). The paired Student's *t* test also was used to compare the SNRs of the acquisitions of images of the left and right median nerves (intrasubject side-to-side variability). The result was a total of 26 comparisons: initial versus second postprocessing for both sides, 12 comparisons; left versus right median nerve for the first and second postprocessing operations, 12 comparisons; and SNR of mean diffusion-weighted direction-encoding and images without diffusion weighting of left versus right median nerves, two comparisons. Thus a Bonferroni-adjusted level of $\alpha = 0.05/26$ comparisons = 0.0019 was considered indicative of significance for all Student's *t* tests [33]. In addition, quantitative data from the first and second postprocessing sessions were averaged to assess the variability among the 15 subjects (intersubject variability) and to calculate Bland-Altman plots of the distribution of differences in quantitative measures between the left and right median nerves.

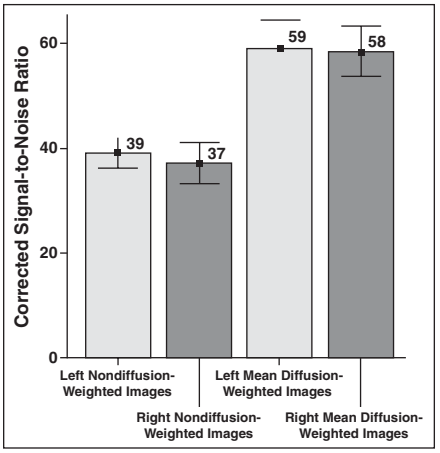

Fig. 4—Bar chart shows equal signal-to-noise ratios of diffusion tensor imaging acquisitions. Bars represent mean corrected signal-to-noise ratios, which were calculated from mean diffusion-weighted images and from reference images without diffusion weighting. Error bars represent mean ± 1.0 standard error.

Results

Precision of Measurement and Fiber Tractography

The average variability between postprocessing sessions was less than 12% with regard to fiber length and less than 5% with regard to determination of FA, ADC, and fiber density index (Table 2). Overall, these differences were not statistically significant (left median nerve, $p = 0.096$–0.586; right median nerve, $p = 0.003$–0.898). On each side, the quality of fiber tract images reconstructed during the initial and subsequent postprocessing operations was rated equal for nine of 15 subjects (60%) and slightly different for six of 15 subjects (40%). None of the fiber tract images reconstructed at the initial postprocessing session was rated very different from its counterpart reconstructed 3 weeks later.

Intersubject Variability

Between subjects, maximum differences of up to 131.5% (left median nerve) and 105.3%

TABLE 3: Maximum Differences in Length of Tracked Fibers, Fiber Density Index, Fractional Anisotropy, and Apparent Diffusion Coefficient (Intersubject Variability) (*n* = 15)

Value	Mean ± SD	Minimum	Maximum	Maximum Difference	
				Maximum – Minimum	%
Left median nerve					
Fiber length (mm)					
Mean	17.1 ± 6.4	9	36	27	300.0
Minimum	8.9 ± 3.5	2	16	14	700.0
Maximum	26.7 ± 13.5	12	71	59	491.7
Fiber density index	31.8 ± 6.9	20.3	47	26.7	131.5
Fractional anisotropy	0.56 ± 0.09	0.43	0.71	0.28	65.1
Apparent diffusion coefficient ($\times 10^{-3}$) (mm^2/s)	1.13 ± 0.13	0.91	1.41	0.5	55.0
Right median nerve					
Fiber length (mm)					
Mean	14.6 ± 4.1	8	23	15	187.5
Minimum	8.9 ± 3.6	4	19	15	375.0
Maximum	20.9 ± 7.9	10	44	34	340.0
Fiber density index	28.8 ± 5.0	21.2	37.7	16.5	77.8
Fractional anisotropy	0.58 ± 0.11	0.38	0.78	0.4	105.3
Apparent diffusion coefficient ($\times 10^{-3}$) (mm^2/s)	1.10 ± 0.17	0.75	1.35	0.6	80.0

Note—All mean ± SD, minimum, and maximum values are means of measurements on two separate occasions ([first postprocessing + second postprocessing] / 2). Percentage difference between minimum and maximum values was calculated as follows: maximum difference = [(maximum value – minimum value)/minimum value] × 100.

(right median nerve) were found for FA, ADC, and fiber density index (Table 3). The maximum difference in mean length of tracked fibers from subject to subject was 300%.

Intrasubject Side-to-Side Variability

Overall, no significant side-to-side difference between the left and the right median nerves was found in the comparisons of length of tracked fibers, FA, ADC, or fiber density index within subjects (first postprocessing, $p = 0.054–0.948$; second postprocessing, $p = 0.056–0.999$). Intrasubject variability was 1.2–30.8% for fiber characteristics and 0–12.5% (mean, 5.1%) for FA, ADC, and fiber density index. Bland-Altman plots were calculated to illustrate the distribution of side-to-side differences between the left and right median nerves (Fig. 3).

The SNRs for the DTI acquisitions of images of the left and the right median nerves were not significantly different ($p = 0.840$, $p = 0.650$). Side-to-side differences were 1.2% and 1.3% for mean diffusion-weighted direction-encoding images and images without diffusion weighting (Fig. 4).

Overall, the quality of fiber tract images of the left median nerve was found to be either slightly or very different from that of the right median nerve. Specifically, the initial postprocessed images of the left and right median nerves of the same subject were qualitatively rated as slightly different for seven of 15 subjects (47%) and as very different for eight of 15 subjects (53%) (Fig. 5). Similar ratings were found for postprocessed images generated 3 weeks later: slightly different for eight of 15 subjects (53%) and very different for seven of 15 subjects (47%).

Discussion

Our study was focused on evaluating intrasubject side-to-side variability in the evaluation of DTI and fiber tractography of the median nerve at the level of the flexor retinaculum (carpal tunnel). As a prerequisite for the evaluation of intrasubject side-to-side variability, we assessed the precision of the image postprocessing (fiber tractography) and quantitative DTI data analysis. Because all operations were performed by the same operator at two different sessions separated from each other by a 3-week interval, this approach can also be interpreted as the determination of intrareader variability. We did not test interreader variability in this study because doing so would require prior standardization of different fiber tractography and quantitative analysis approaches to peripheral nerve DTI.

We found less than 5% intrareader variability in FA, ADC, and fiber density index measurements. Measurements of fiber length, however, were slightly less precise (< 12% variability), but the difference was not statistically significant. These observations are in good agreement with our findings on image quality. Both readers rated all fiber tract images produced at either postprocessing session as equal or as only slightly different. Because our study was the first, to the best of our knowledge, in which the precision of quantitative DTI and fiber tractography evaluation was systematically assessed in the peripheral nervous system, there are no data in the literature available for comparison. From corresponding studies of the brain, it is known that imprecise ROI placement is as a major source of intrareader variability [27]. We used the same data sets for analysis and the same parameters for postprocessing. Thus the only source of the intrareader variability observed in our study is ROI placement. Further precision studies are needed to determine the optimal anatomic landmarks for ROI placement in peripheral nerves to achieve highest precision of quantitative measurements.

We found no statistically significant side-to-side differences in quantitative data when we evaluated the left and the right median nerves. Maximal intrasubject side-to-side variability was up to approximately 31% for, for example, the maximum length of reconstructed fibers. This observation may explain the finding that both radiologists rated images of the left and right sides as slightly different or very different for all subjects. Both radiologists tended to overvalue the criterion maximum fiber length compared with the other criteria, such as fiber tract order and homogeneity, fiber tract organization, appearance of fiber bundles in boundary regions, and apparent density of fiber bundles.

Smaller intrasubject side-to-side variability of less than 12.5% was observed for FA, ADC, and fiber density index measurements. This finding may be explained by the fact that FA, ADC, and fiber density index measurements depend on placing ROIs within the median nerve in a specific transaxial plane. In our study, all measurements were performed at the level of the flexor retinaculum (hook of

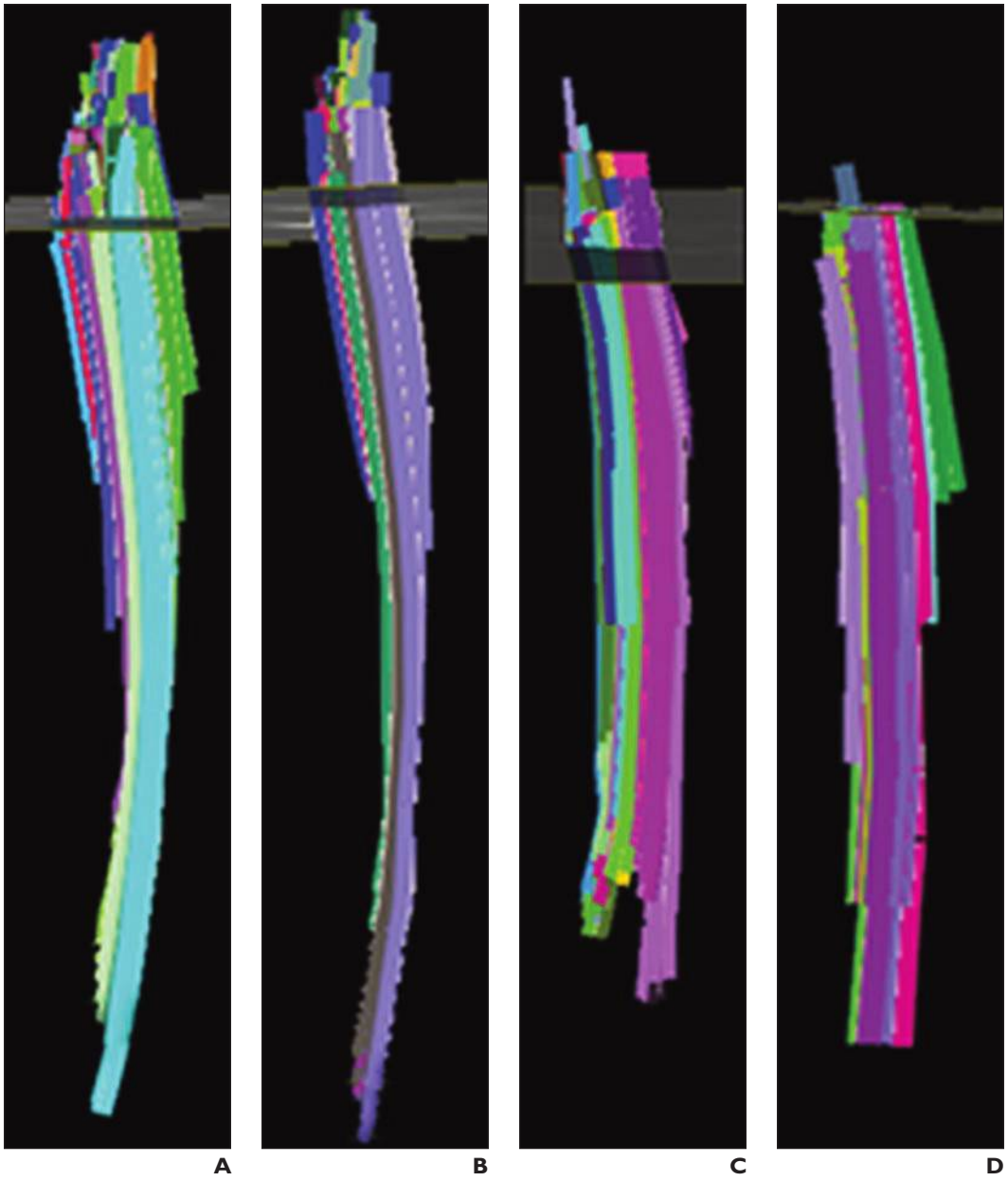

Fig. 5—32-year-old healthy man. **A** and **B,** Fiber tract images generated during initial postprocessing (**A**) of diffusion tensor imaging and at postprocessing 3 weeks later (**B**) show fibers tracked through regions of interest in left median nerve.
C and **D,** Fiber tract images generated during initial postprocessing (**C**) of diffusion tensor imaging and at postprocessing 3 weeks later (**D**) show fibers tracked through regions of interest in right median nerve.

hamate). On the basis of observed mean side-to-side variabilities of 5.1% for FA, ADC, and fiber density index, this finding seems to represent a good anatomic landmark allowing reliable quantitative DTI data evaluation. This landmark also was used in a study by Kabakci et al. [17], in which normative diffusion values were reported in a cohort of 20 healthy volunteers. Considering the slightly different imaging and reconstruction parameters in our study compared with the previous investigation, our FA and ADC data are in very good agreement with the corresponding data of Kabakci et al., who reported FA values of 0.59 ± 0.07 and ADC values of 0.97 ± 0.03 × 10^{-3} mm^2/s for the median nerve. However, results in that study showed fairly large intersubject variability, FA ranging from 0.50 to 0.73 (maximum difference, 46%) and ADC ranging from 0.43 to 1.61 × 10^{-3} mm^2/s (maximum difference, 274%).

We found large intersubject variability, which hampers the use of normative values gained from intersubject studies in the diagnosis of peripheral neuropathy, such as carpal tunnel syndrome. Therefore, we recommend imaging the contralateral side as an internal control in all patients for whom DTI is used in the evaluation of unilateral peripheral neuropathy [34]. Our findings suggest use of a variability cutoff value of 5%. This practice would mean that in clinical practice, side-to-side differences greater than 5% might be attributed to disease. Although we acknowledge that in some conditions, such as carpal tunnel syndrome, the contralateral structure can frequently be affected, normative values gained from the same subjects would potentially allow defining ranges of abnormal FA and ADC values in future research, which might be focused on purely unilateral pathologic conditions of peripheral nerves. Our recommendation, however, applies only to quantitative evaluation of DTI rather than to fiber tractography. Side-to-side differences in fiber tract image quality

were remarkable in our study. Therefore, fiber tract images of the right and left median nerves should not be compared with each other, and potential differences in fiber tract images should not be considered abnormal, such as during reporting of patient findings.

Our investigation confirmed that noise effects, which can be a cause of systematic measurement errors at DTI, can be eliminated as a source of side-to-side variability of FA and ADC. No significant side-to-side differences in SNR were observed in our study. This finding was expected because we used the same hardware and the same imaging protocol to image both wrists.

Our study was limited by the small number of subjects and the fact that the study sample does not represent clinical practice. It may be possible that greater intrasubject variability exists among elderly persons. Future studies should be performed to investigate the age dependency of DTI measures. Another limitation was that the postprocessing software is not standardized, and different fiber reconstruction algorithms are used (the software used in this study entails a powerful so-called brute-force algorithm) [4, 35]. Thus even when the same DTI data set would yield the same absolute number of tracked fibers, fiber length and fiber density index might be different with different software.

Our preliminary results indicate that quantitative evaluation of DTI of the median nerve is precise. The absence of statistically significant intrasubject side-to-side variability in quantitative data suggests that the healthy contralateral nerve can be used as an internal control. The observed side-to-side variability in the quality of fiber tract images rules out side-to-side comparisons in fiber tractography.

References

1. Mori S, van Zijl PC. Fiber tracking: principles and strategies: a technical review. *NMR Biomed* 2002; 15:468–480
2. Mori S, Barker PB. Diffusion magnetic resonance imaging: its principle and applications. *Anat Rec* 1999; 257:102–109
3. Bammer R. Basic principles of diffusion-weighted imaging. *Eur J Radiol* 2003; 45:169–184
4. Bammer R, Acar B, Moseley ME. In vivo MR tractography using diffusion imaging. *Eur J Radiol* 2003; 45:223–234
5. Nucifora PG, Verma R, Lee SK, Melhem ER. Diffusion-tensor MR imaging and tractography: exploring brain microstructure and connectivity. *Radiology* 2007; 245:367–384
6. Mori S, Zhang J. Principles of diffusion tensor imaging and its applications to basic neuroscience research. *Neuron* 2006; 51:527–539
7. Landman BA, Farrell JA, Jones CK, Smith SA, Prince JL, Mori S. Effects of diffusion weighting schemes on the reproducibility of DTI-derived fractional anisotropy, mean diffusivity, and principal eigenvector measurements at 1.5T. *Neuroimage* 2007; 36:1123–1138
8. Lee SK, Kim DI, Kim J, et al. Diffusion-tensor MR imaging and fiber tractography: a new method of describing aberrant fiber connections in developmental CNS anomalies. *RadioGraphics* 2005; 25:53–65; discussion 66–58
9. Schaefer PW, Copen WA, Lev MH, Gonzalez RG. Diffusion-weighted imaging in acute stroke. *Magn Reson Imaging Clin N Am* 2006; 14:141–168
10. Ducreux D, Fillard P, Facon D, et al. Diffusion tensor magnetic resonance imaging and fiber tracking in spinal cord lesions: current and future indications. *Neuroimaging Clin N Am* 2007; 17:137–147
11. Ozanne A, Krings T, Facon D, et al. MR diffusion tensor imaging and fiber tracking in spinal cord arteriovenous malformations: a preliminary study. *Am J Neuroradiol* 2007; 28:1271–1279
12. Sugiyama K, Kondo T, Higano S, et al. Diffusion tensor imaging fiber tractography for evaluating diffuse axonal injury. *Brain Inj* 2007; 21:413–419
13. Rollins NK. Clinical applications of diffusion tensor imaging and tractography in children. *Pediatr Radiol* 2007; 37:769–780
14. Chen X, Weigel D, Ganslandt O, Buchfelder M, Nimsky C. Diffusion tensor imaging and white matter tractography in patients with brainstem lesions. *Acta Neurochir (Wien)* 2007; 149:1117–1131; discussion 1131
15. Chen X, Weigel D, Ganslandt O, Fahlbusch R, Buchfelder M, Nimsky C. Diffusion tensor-based fiber tracking and intraoperative neuronavigation for the resection of a brainstem cavernous angioma. *Surg Neurol* 2007; 68:285–291; discussion 291
16. Jiang H, van Zijl PC, Kim J, Pearlson GD, Mori S. dtiStudio: resource program for diffusion tensor computation and fiber bundle tracking. *Comput Methods Programs Biomed* 2006; 81:106–116
17. Kabakci N, Gurses B, Firat Z, et al. Diffusion tensor imaging and tractography of median nerve: normative diffusion values. *AJR* 2007; 189:923–927
18. Skorpil M, Engstrom M, Nordell A. Diffusion-direction-dependent imaging: a novel MRI approach for peripheral nerve imaging. *Magn Reson Imaging* 2007; 25:406–411
19. Tsuchiya K, Fujikawa A, Tateishi H, Nitatori T. Visualization of cervical nerve roots and their distal nerve fibers by diffusion-weighted scanning using parallel imaging. *Acta Radiol* 2006; 47:599–602
20. Meek MF, Stenekes MW, Hoogduin HM, Nicolai JP. In vivo three-dimensional reconstruction of human median nerves by diffusion tensor imaging. *Exp Neurol* 2006; 198:479–482
21. Hiltunen J, Suortti T, Arvela S, Seppa M, Joensuu R, Hari R. Diffusion tensor imaging and tractography of distal peripheral nerves at 3 T. *Clin Neurophysiol* 2005; 116:2315–2323
22. Skorpil M, Karlsson M, Nordell A. Peripheral nerve diffusion tensor imaging. *Magn Reson Imaging* 2004; 22:743–745
23. Khalil C, Hancart C, Le Thuc V, Chantelot C, Chechin D, Cotten A. Diffusion tensor imaging and tractography of the median nerve in carpal tunnel syndrome: preliminary results. *Eur Radiol* 2008; 18:2283–2291
24. Yao L, Gai N. Median nerve cross-sectional area and MRI diffusion characteristics: normative values at the carpal tunnel. *Skeletal Radiol* 2009; 38: 355–361
25. Wakana S, Caprihan A, Panzenboeck MM, et al. Reproducibility of quantitative tractography methods applied to cerebral white matter. *Neuroimage* 2007; 36:630–644
26. Farrell JA, Landman BA, Jones CK, et al. Effects of signal-to-noise ratio on the accuracy and reproducibility of diffusion tensor imaging-derived fractional anisotropy, mean diffusivity, and principal eigenvector measurements at 1.5 T. *J Magn Reson Imaging* 2007; 26:756–767
27. Bonekamp D, Nagae LM, Degaonkar M, et al. Diffusion tensor imaging in children and adolescents: reproducibility, hemispheric, and age-related differences. *Neuroimage* 2007; 34:733–742
28. Muller MJ, Mazanek M, Weibrich C, Dellani PR, Stoeter P, Fellgiebel A. Distribution characteristics, reproducibility, and precision of region of interest-based hippocampal diffusion tensor imaging measures. *Am J Neuroradiol* 2006; 27:440–446
29. Andreisek G, White LM, Kassner A, Tomlinson G, Sussman MS. Diffusion tensor imaging and fiber tractography of the median nerve at 1.5T: optimization of b value. *Skeletal Radiol* 2009; 38:51–59
30. Roberts TP, Liu F, Kassner A, Mori S, Guha A. Fiber density index correlates with reduced fractional anisotropy in white matter of patients with glioblastoma. *Am J Neuroradiol* 2005; 26:2183–2186
31. Dietrich O, Heiland S, Sartor K. Noise correction for the exact determination of apparent diffusion coefficients at low SNR. *Magn Reson Med* 2001; 45:448–453
32. Henkelman RM. Measurement of signal intensities in the presence of noise in MR images. *Med Phys* 1985; 12:232–233
33. Tello R, Crewson PE. Hypothesis testing. Part 2. Means. *Radiology* 2003; 227:1–4
34. Andreisek G, Crook DW, Burg D, Marincek B, Weishaupt D. Peripheral neuropathies of the median, radial, and ulnar nerves: MR imaging features. *RadioGraphics* 2006; 26:1267–1287
35. Masutani Y, Aoki S, Abe O, Hayashi N, Otomo K. MR diffusion tensor imaging: recent advance and new techniques for diffusion tensor visualization. *Eur J Radiol* 2003; 46:53–66

This article has been cited by:

1. Lukas Filli, Marco Piccirelli, David Kenkel, Andreas Boss, Andrei Manoliu, Gustav Andreisek, Himanshu Bhat, Val M. Runge, Roman Guggenberger. 2015. Accelerated magnetic resonance diffusion tensor imaging of the median nerve using simultaneous multi-slice echo planar imaging with blipped CAIPIRINHA. *European Radiology* . [CrossRef]
2. Yin Shi, Min Zong, Xiaoquan Xu, Yuefen Zou, Yang Feng, Wei Liu, Chuanbing Wang, Dehang Wang. 2015. Diffusion tensor imaging with quantitative evaluation and fiber tractography of lumbar nerve roots in sciatica. *European Journal of Radiology* **84**, 690-695. [CrossRef]
3. Haci Taner Bulut, Adem Yildirim, Burcu Ekmekci, Hediye Pinar Gunbey. 2014. The Diagnostic and Grading Value of Diffusion Tensor Imaging in Patients with Carpal Tunnel Syndrome. *Academic Radiology* **21**, 767-773. [CrossRef]
4. Yuxiang Zhou, Ponnada A. Narayana, Manickam Kumaravel, Parveen Athar, Vipulkumar S. Patel, Kazim A. Sheikh. 2014. High resolution diffusion tensor imaging of human nerves in forearm. *Journal of Magnetic Resonance Imaging* **39**:10.1002/jmri.v39.6, 1374-1383. [CrossRef]
5. Marianna Brienza, Francesco Pujia, M. Chiara Colaiacomo, M. Grazia Anastasio, Francesco Pierelli, Claudio Di Biasi, Chiara Andreoli, Gianfranco Gualdi, Gabriele O.R. Valente. 2014. 3T diffusion tensor imaging and electroneurography of peripheral nerve: A morphofunctional analysis in carpal tunnel syndrome. *Journal of Neuroradiology* **41**, 124-130. [CrossRef]
6. Boklye Kim, Ashok Srinivasan, Brian Sabb, Eva L Feldman, Rodica Pop-Busui. 2014. Diffusion Tensor Imaging of the Sural Nerve in normal controls. *Clinical Imaging* . [CrossRef]
7. Sung Yoon Park, Chan Kyo Kim, Byung Kwan Park, Sang Yun Ha, Ghee Young Kwon, Bohyun Kim. 2014. Diffusion-Tensor MRI at 3 T: Differentiation of Central Gland Prostate Cancer From Benign Prostatic Hyperplasia. *American Journal of Roentgenology* **202**:3, W254-W262. [Abstract] [Full Text] [PDF] [PDF Plus]
8. Yue-Yao Chen, Xiao-Feng Lin, Fang Zhang, Xiang Zhang, Hui-Jun Hu, Dong-Ye Wang, Lie-Jing Lu, Jun Shen. 2014. Diffusion Tensor Imaging of Symptomatic Nerve Roots in Patients with Cervical Disc Herniation. *Academic Radiology* **21**, 338-344. [CrossRef]
9. Gaurav K. Thawait, Avneesh Chhabra, John A. Carrino, John Eng. 2014. Magnetic Resonance Neurography Research. *Neuroimaging Clinics of North America* **24**, 257-261. [CrossRef]
10. Avneesh Chhabra, Aaron Flammang, Abraham Padua, John A. Carrino, Gustav Andreisek. 2014. Magnetic Resonance Neurography. *Neuroimaging Clinics of North America* **24**, 67-78. [CrossRef]
11. Patrick Eppenberger, Gustav Andreisek, Avneesh Chhabra. 2014. Magnetic Resonance Neurography. *Neuroimaging Clinics of North America* **24**, 245-256. [CrossRef]
12. Ali Naraghi, Lucas da Gama Lobo, Ravi Menezes, Monica Khanna, Marshall Sussman, Dimitri Anastakis, Lawrence M. White. 2013. Diffusion tensor imaging of the median nerve before and after carpal tunnel release in patients with carpal tunnel syndrome: feasibility study. *Skeletal Radiology* **42**, 1403-1412. [CrossRef]
13. B. Dallaudière, J. Lincot, A. Hess, V. Balbi, F. Cornelis, A. Larbi, J.-P. Laissy, A. Cotten, É. Schouman-Claeys. 2013. Intérêt clinique des paramètres d'imagerie de tenseur de diffusion dans les conflits disco-radiculaires lombaires. *Journal de Radiologie Diagnostique et Interventionnelle* . [CrossRef]
14. B. Dallaudière, J. Lincot, A. Hess, V. Balbi, F. Cornelis, A. Larbi, J.-P. Laissy, A. Cotten, E. Schouman-Claeys. 2013. Clinical relevance of diffusion tensor imaging parameters in lumbar disco-radicular conflict. *Diagnostic and Interventional Imaging* . [CrossRef]
15. Yasar Altun, Murat Serhat Aygun, Mehmet Ugur Cevik, Abdullah Acar, Sefer Varol, Adalet Arıkanoglu, Hakan Onder, Ertugrul Uzar. 2013. Relation between electrophysiological findings and diffusion weighted magnetic resonance imaging in ulnar neuropathy at the elbow. *Journal of Neuroradiology* **40**, 260-266. [CrossRef]
16. Keith A. Cauley, Christopher G. Filippi. 2013. Diffusion-Tensor Imaging of Small Nerve Bundles: Cranial Nerves, Peripheral Nerves, Distal Spinal Cord, and Lumbar Nerve Roots— Clinical Applications. *American Journal of Roentgenology* **201**:2, W326-W335. [Abstract] [Full Text] [PDF] [PDF Plus]
17. Roman Guggenberger, Daniel Nanz, Lorenz Bussmann, Avneesh Chhabra, Michael A. Fischer, Jürg Hodler, Christian W.A. Pfirrmann, Gustav Andreisek. 2013. Diffusion tensor imaging of the median nerve at 3.0T using different MR scanners: Agreement of FA and ADC measurements. *European Journal of Radiology* . [CrossRef]
18. Lianxin Zhao, Guangbin Wang, Linlin Yang, Lebin Wu, Xiangtao Lin, Avneesh Chhabra. 2013. Diffusion-Weighted MR Neurography of Extremity Nerves With Unidirectional Motion-Probing Gradients at 3 T: Feasibility Study. *American Journal of Roentgenology* **200**:5, 1106-1114. [Abstract] [Full Text] [PDF] [PDF Plus]

19. Avneesh Chhabra. 2013. Magnetic Resonance Neurography—Simple Guide to Performance and Interpretation. *Seminars in Roentgenology* **48**, 111-125. [CrossRef]
20. Avneesh Chhabra, Lianxin Zhao, John A. Carrino, Eo Trueblood, Saso Koceski, Filip Shteriev, Lionel Lenkinski, Christopher D. J. Sinclair, Gustav Andreisek. 2013. MR Neurography: Advances. *Radiology Research and Practice* **2013**, 1-14. [CrossRef]
21. Bruno Grignon, Laurence Mainard, Matthieu Delion, Claude Hodez, Guillaume Oldrini. 2012. Recent advances in medical imaging: anatomical and clinical applications. *Surgical and Radiologic Anatomy* **34**, 675-686. [CrossRef]
22. Roman Guggenberger, Daniel Markovic, Patrick Eppenberger, Avneesh Chhabra, Andreas Schiller, Daniel Nanz, Klaas Prüssmann, Gustav Andreisek. 2012. Assessment of Median Nerve with MR Neurography by Using Diffusion-Tensor Imaging: Normative and Pathologic Diffusion Values. *Radiology* **265**, 194-203. [CrossRef]
23. M. Ohana, T. Moser, N. Meyer, P.E. Zorn, P. Liverneaux, J.-L. Dietemann. 2012. 3T tractography of the median nerve: Optimisation of acquisition parameters and normative diffusion values. *Diagnostic and Interventional Imaging* **93**, 775-784. [CrossRef]
24. Yuxiang Zhou, Manickam Kumaravel, Vipulkumar S. Patel, Kazim A. Sheikh, Ponnada A. Narayana. 2012. Diffusion tensor imaging of forearm nerves in humans. *Journal of Magnetic Resonance Imaging* **36**:10.1002/jmri.v36.4, 920-927. [CrossRef]
25. M. Ohana, T. Moser, N. Meyer, P.-E. Zorn, P. Liverneaux, J.-L. Dietemann. 2012. Tractographie du nerf médian à 3T : optimisation des paramètres d'acquisition et mesure des paramètres de diffusivité. *Journal de Radiologie Diagnostique et Interventionnelle* **93**, 822-831. [CrossRef]
26. Ammar Mallouhi, Wolfgang Marik, Daniela Prayer, Franz Kainberger, Gerd Bodner, Gregor Kasprian. 2012. 3T MR tomography of the brachial plexus: Structural and microstructural evaluation. *European Journal of Radiology* **81**, 2231-2245. [CrossRef]
27. Roman Guggenberger, Daniel Nanz, Gilbert Puippe, Kaspar Rufibach, Lawrence M. White, Marshall S. Sussman, Gustav Andreisek. 2012. Diffusion tensor imaging of the median nerve: intra-, inter-reader agreement, and agreement between two software packages. *Skeletal Radiology* **41**, 971-980. [CrossRef]
28. Jaana Hiltunen, Erika Kirveskari, Jussi Numminen, Nina Lindfors, Harry Göransson, Riitta Hari. 2012. Pre- and post-operative diffusion tensor imaging of the median nerve in carpal tunnel syndrome. *European Radiology* **22**, 1310-1319. [CrossRef]
29. Ty K. Subhawong, Kenneth C. Wang, Shrey K. Thawait, Eric H. Williams, Shahreyar Shar Hashemi, Antonio J. Machado, John A. Carrino, Avneesh Chhabra. 2012. High resolution imaging of tunnels by magnetic resonance neurography. *Skeletal Radiology* **41**, 15-31. [CrossRef]
30. Alberto Tagliafico, Massimo Calabrese, Matteo Puntoni, Daniele Pace, Gabriella Baio, Carlo Emanuele Neumaier, Carlo Martinoli. 2011. Brachial plexus MR imaging: accuracy and reproducibility of DTI-derived measurements and fibre tractography at 3.0-T. *European Radiology* **21**, 1764-1771. [CrossRef]